Journal of Energy Storage 13 (2017) 378–386

Contents lists available at ScienceDirect

Journal of Energy Storage

journal homepage: www.elsevier.com/locate/est

Overcharge and thermal destructive testing of lithium metal oxide and lithium metal phosphate batteries incorporating optical diagnostics

Frank Austin Mier[a,*], Rudy Morales[a], Caralyn A. Coultas-McKenney[a], Michael J. Hargather[a,*], Jason Ostanek[b,1]

[a] New Mexico Tech, Socorro, NM 87801, United States
[b] Naval Surface Warfare Center Philadelphia Division, Philadelphia, PA 19112, United States

ARTICLE INFO

Article history:
Received 30 January 2017
Received in revised form 21 June 2017
Accepted 14 August 2017
Available online 9 October 2017

Keywords:
Lithium batteries
Destructive testing
Overcharge
Schlieren imaging

ABSTRACT

Lithium batteries have a tendency to fail violently under adverse conditions leading to the rapid venting of gas. Overcharge, thermal heating, and a combination of the two conditions are applied here to investigate the gas venting process. A test chamber has been constructed with data recordings including chamber pressure and temperature, battery voltage, current, and surface temperature as functions of time throughout the charging and failure processes. High-speed imaging and schlieren flow visualization are used to visualize the gas venting process. A direct comparison between lithium iron phosphate based K2 26650 and lithium nickel manganese cobalt oxide LG 18650 cells is made through a test series of the three failure methods. Failure under thermal, overcharge, and thermal-overcharge conditions are generally similar in terms of the gas venting process, but are observed to have increasingly energetic failures. The thermal-overcharge abuse condition demonstrates an ability to reconnect via internal short circuit even after an initial electrical failure seen as the refusal to accept charge. This reconnection is associated with a secondary, more energetic failure which can produce weak shock pressure waves.

1. Introduction

Lithium batteries provide a high energy density source which has been applied to most portable applications. Such a concentration of stored electrochemical energy generally involves significant risks in the cases of end user abuse, unexpected loading conditions, design flaws, or manufacturing defects. Examples of lithium battery failures including combustion in popular smartphones and commercial airliners have brought much attention to these hazards [1,2]. With popular uses such as personal electronics and electric vehicle transportation, it is important to understand the failures of these components such that risks can be minimized.

Commercially available lithium secondary cells generally contain one or more different protective devices to minimize the risk from inherently hazardous chemistries. Current interrupt devices (CID) protect during overcharge scenarios by physically separating the cathode from the circuit [3]. Positive temperature coefficient (PTC) devices temporarily protect against thermal loading via increasing resistance. Thermal fuses can also provide protection from excess temperature by permanently or temporarily disconnecting the circuit. Many batteries, including the ones tested here, have vents which allow for the release of gases which can build to dangerous pressure levels, leaving the battery permanently damaged. Separator shutdown provides protection by inhibiting ion transport when the temperature within the cell exceeds the melting point of the separator. If the separator further increases in temperature, it can eventually melt causing violent reactions [4].

The most commercially prevalent group of lithium battery chemistries contain layered, lithium metal oxide cathodes. Examples of this group are lithium cobalt oxide (LCO), lithium nickel manganese cobalt oxide (NMC), and lithium nickel cobalt aluminum oxide (NCA). Under overcharge conditions, cathode decomposition results in generation of oxygen gas and lithium ions [5]. Additionally, intercalated lithium within the electrolyte can react resulting in formation of hydrocarbons [6]. The presence of both oxygen and hydrocarbons presents a significant flammability risk. Research has been done to introduce new chemistries which are cost effective, higher energy density, and inherently more safe. Lithium iron phosphate (LFP) has been presented as thermally

* Corresponding authors.
E-mail addresses: frank.mier@student.nmt.edu (F.A. Mier), michael.hargather@nmt.edu (M.J. Hargather).
[1] Current address: Purdue University, West Lafayette, IN 47907, United States.

http://dx.doi.org/10.1016/j.est.2017.08.003
2352-152X/

stable alternative with a more level discharge voltage curve than lithium cobalt oxide, but it performs at somewhat lower voltage [7]. However, vented cell material analyzed from LCO, NMC, and LFP cells contains hydrogen gas which can present safety concerns [8]. An alternative sodium based chemistry (Na_xFePO_4F) has also shown promise which would be cost effective and less hazardous [9].

Modeling and testing of lithium cells show trends and hazards during battery failures. Numerical models have been created for thermal testing of cells and have shown significant improvement in correlations to experimental data with venting considerations under isentropic flow assumptions [10]. Testing inside an adiabatic calorimeter has shown a relationship between time to failure and state of charge (SOC) in thermal testing which provides data on temperature and pressure [11]. Cone calorimetry tests have also shown the relationship between time to failure and SOC while also showing combustion of 18650 format cells [12]. Thermal imaging and high-speed tomography have shown how specific components of cells breakdown and lead to thermal runaway [13].

Measurements of the external flow associated with battery venting are underdeveloped. Incorporation of high-speed schlieren imaging can visualize refractive gradients in gases associated with chemical species and density variation [14]. This experimental technique can also be used to image pressure and shock wave propagation [15] which could cause undesirable pressure-loading on cells adjacent to a failing cell. The test facility presented here integrates imaging with other common measurements such as voltage, current, temperature, and pressure to provide broad measurements throughout the failure process. The ability to test overcharge and thermal failure conditions allows for a variety of test conditions allowing for test of situations otherwise unexplored.

2. Battery test facility

2.1. Test chamber

A laboratory facility was constructed for the testing, containment, and data collection of lithium battery failures. The facility design focused on creating a reusable and modular enclosure for testing, with instrumentation and remote test operation capabilities. The test chamber, along with all associated electrical systems, are mounted on top of an optical table measuring approximately 2 m by 6 m in a room separated from test operators. An annotated image of the laboratory setup is shown in Fig. 1.

The test chamber is a vessel with four viewing windows and seven ports for overcharge wiring, instrumentation, and air lines for post-test chamber purge. The chamber is a single 254 mm square by 762 mm long steel square tube with 9.5 mm wall thickness. Batteries are aligned with the tube allowing for an axial viewing window on the end of the chamber which is 235 mm square. Side windows viewing perpendicularly to the length of battery cells have a viewing area of 152 mm high and 406 mm wide. All windows are constructed from 12.7 mm thick acrylic which are laser cut and can be easily replaced if damaged during testing. Rubber gaskets and a 12.7 mm thick A36 steel frame which is bolted directly to the chamber provide secure mounting and sealing of the windows.

The interior of the containment chamber is coated with an electrical insulator to isolate batteries as the test chamber structure itself is connected to ground. An anodized optical breadboard is secured to the bottom of the vessel to allow for versatile mounting options. An acrylic cover is placed directly on top of the optical breadboard to minimize possible short circuits between the overcharge circuit positive lead in case of separation from the battery during testing.

Ports allow for instrumentation, purge, and overcharge wiring to be placed within the chamber. The locations and uses for all ports are shown in Fig. 1. Instrumentation crossing into the sealed environment within the chamber includes a piezoelectric pressure transducer (PCB Piezotronics Model 102B15) to measure dynamic pressure, a pressure transducer (Wika Model A10) for static pressure, K-type thermocouples for surface (Omega 5TC-GG-K-24-36) and air temperature (Omega KTSS-14E-6). On opposite side walls of the chamber, two ports are fitted with airtight cord grips allowing for the insulated 4/0 gauge wire leads of the overcharge system. The majority of ports located on the test chamber use a gusset plate with a standard bolt pattern and a matching gasket for simplification of maintenance and reconfiguration. An example such is the addition of a 120 V_{AC} line through port used to measure battery surface temperature. This is necessary on thermal and combination testing. Gusset plates all have a central tapped hole for the appropriate instrument, purge tube, or overcharge line. These plates use NPT standard tapered threads to maintain appropriate seal.

The port for the piezoelectric pressure transducer is flush-mounted to the test chamber such that the diaphragm is coplanar with the top wall of the test chamber to accurately measure the dynamic pressure during battery failures. A 1.65 mm recessed area was milled into the top of the chamber and 3/8-24 UNC tapped through hole allowing the pressure transducer to be threaded to the proper depth and held against a rubber gasket.

The purge system consists of an entrance on the top of the chamber directly above the battery cells and an exit located near the bottom of the chamber on a side wall adjacent to one of the end windows. Gusset plates on the ports connect to Swagelok brand tube fittings using 12.7 mm stainless steel tube. Electrically actuated ball valves are connected to the ends of these tubes, so

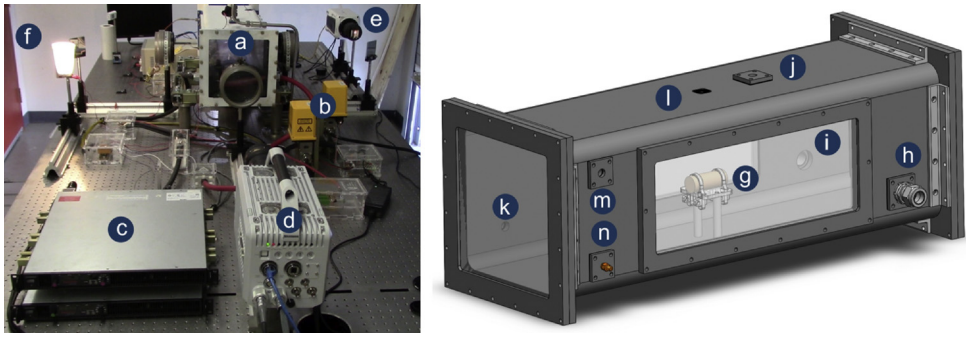

Fig. 1. Left is a photograph of the installed laboratory setup with the (a) test chamber, (b) purge valves, (c) power supplies, (d) axial camera (Photron SA-X2 shown), and (e) side camera (Phantom v711 shown). Test operators are located behind the (f) door. Right is a model of the test chamber with annotated locations for the (g) battery, (h–i) overcharge wiring, (j) purge inlet, (k) purge outlet, (l) piezoelectric pressure transducer, (m) air temperature probe, and (n) surface temperature thermocouple.